Astron. Astrophys. 342, 799–808 (1999)

ASTRONOMY AND ASTROPHYSICS

SiO rotation-vibration bands in cool giants⋆

II. The behaviour of SiO bands in AGB stars

B. Aringer[1], **S. Höfner**[2], **G. Wiedemann**[3], **J. Hron**[1], **U.G. Jørgensen**[2], **H.U. Käufl**[3], **and W. Windsteig**[1]

[1] Institut für Astronomie der Universität Wien, Türkenschanzstrasse 17, A-1180 Wien, Austria
(e-mail: aringer/hron/windsteig@astro.astro.univie.ac.at)
[2] Astronomisk Observatorium, Københavns Universitet, Juliane Maries Vej 30, DK-2100 Copenhagen, Denmark
(e-mail: hoefner/uffegj@stella.nbi.dk)
[3] European Southern Observatory, Karl-Schwarzschild-Strasse 1, D-85748 Garching bei München, Germany
(e-mail: gwiedema/hukaufl@eso.org)

Received 5 June 1998 / Accepted 30 October 1998

Abstract. The first overtone rotation-vibration transitions of SiO give rise to prominent bandheads in the wavelength range between 4.0 and $4.5\,\mu$m. In order to study the behaviour of these features in AGB stars we observed the 3.94 to $4.12\,\mu$m spectra for a sample of 23 oxygen-rich late-type variables. In contrast to the SRb objects, the Miras show a very large scatter of the equivalent widths of the SiO bands. Despite their cool temperatures some of them have only weak or no SiO absorption, which seems to be related to their strong pulsations producing a large variability of the features. When comparing the band intensities with photometric data, we found a general decrease with bluer IRAS $(12-25)$ colors. However, this trend may only reflect the different behaviour of the Miras and SRb stars in our sample. We did not discover any correlation of the equivalent widths with the effective temperatures derived from $(J-K)$, or with the $(K-12)$ color and the IRAS-LRS class, both of which can be regarded as a rough measure for the thickness of the circumstellar shell.

In Paper I of this series (Aringer et al. 1997a) we have shown that synthetic spectra calculated from hydrostatic MARCS atmospheres are successful in reproducing the observed band intensities of giants with spectral types earlier than about M5 III and M2 II. However, they generally predict too strong features for very cool and extended objects, as they are discussed in this work. And they fail completely when it comes to Miras with weak or no SiO absorption. These stars are dominated by dynamical phenomena and, not surprisingly, they can therefore not be described by hydrostatic structures. Thus, we have also computed synthetic spectra based on experimental dynamical models. Although they still have some shortcomings, we demonstrate that, in principle, they are able to explain the whole range of equivalent widths of the observed SiO bandheads and their variations.

Key words: infrared: stars – stars: AGB and post-AGB – stars: late-type – stars: fundamental parameters – stars: atmospheres

1. Introduction

Together with H_2 and CO, SiO is one of the most abundant molecules in the atmospheres of oxygen-rich AGB stars. It is also regarded to be the prime condensate for the silicate dust that is formed around these objects (Gail & Sedlmayr 1986). Several features in the infrared and radio spectra of late-type stars are produced by SiO, probing quite different regions in their atmospheres and circumstellar shells.

The band system generated by the first overtone rotation-vibration transitions is situated in the near infrared. It is formed in the "photosphere" (= deeper atmospheric layers with $T > 2000\,$K), which is, especially in cool Mira variables dominated by stellar pulsations and related shock waves. This band system is particularly interesting, since its short wavelength end at $4\,\mu$m can easily be observed with ground based telescopes (e.g. Rinsland & Wing 1982, Aringer et al. 1995) and is not contaminated with emission or absorption caused by other molecules (except some water absorption in very cool stars). For some of the brighter AGB stars there are also high resolution Fourier-transform spectra available (Ridgway et al. 1984, Tsuji et al. 1994). In contrast to the fundamental band system situated around $8\,\mu$m the first overtone transitions do not interfere with the strong dust features produced by the circumstellar shells of many AGB stars.

In Paper I of this series (Aringer et al. 1997a, Paper I) we have published a large grid of synthetic SiO spectra calculated from hydrostatic MARCS atmospheres. They cover the range between 2.0 and 12.5 μm at a very low resolution of about 50 and the region of the first overtone bandheads around 4 μm at a medium resolution of 4000. We have investigated the behaviour of the SiO features as a function of different stellar parameters like temperature, log (g), stellar mass and metallicity, and we have compared our results to existing observations. One of the

Send offprint requests to: B. Aringer

⋆ Based on observations made at the European Southern Observatory (ESO), La Silla (Chile)

conclusions of Paper I was that the appearance of the SiO bands in giants with $T_{\rm eff} > 3600$ K (K and early M) could be very well explained by our models, while they tend to predict too intense absorption features for the cooler and more extended stars. This problem has also been discussed by Tsuji et al. (1994), who proposed a "warm molecular envelope" (Tsuji et al. 1997) in order to remove the discrepancies. However, it should be mentioned in this context that one may not expect that the atmospheres of AGB variables showing such phenomena as pulsation connected with shock waves, heavy mass loss and dust formation can be described by hydrostatic models.

This topic will be discussed in the current paper where we will focus on our own observations of AGB stars (see also Aringer et al. 1995) and synthetic spectra based on dynamical model atmospheres as they have been computed by Höfner & Dorfi (1997). A similar method to reproduce the observations of carbon-rich objects has been applied by Loidl et al. (1997) and Hron et al. (1998).

2. Observations

In order to study the first overtone rotation-vibration bandheads of SiO we observed the spectral range from 3.94 to $4.12\,\mu$m for a sample of 23 oxygen-rich late-type giants, most of which are Mira or Semiregular (SR) variables. Also two Irregular variables have been included. The sources have been selected due to their variability types, their bright L-magnitude (< 1.5), the existence of reliable JHKLM as well as IRAS 12 and $25\,\mu$m photometry and the existence of a good IRAS-LRS spectrum. As it is shown in Table 1 the stars cover a large variety of photometric periods and infrared colors. Due to their pulsational properties at least most of them are expected to be situated on the AGB (e.g. Alvarez et al. 1997).

The spectra have been observed in June 1993 with the cooled grating spectrograph IRSPEC at the ESO NTT and reduced with MIDAS. They are composed of 5 overlapping parts corresponding to different grating positions. The final resolution is approximately 4000. To eliminate atmospheric features and effects of detector response, spectra of nearby O and B stars were taken at the same time and included into the reduction. The hot objects were mainly used for the determination of the stellar continua, since, apart from Brackett-α, they do not show any distinct features in the studied wavelength range. However, concerning the overall slopes of the measured energy distributions we did not always get consistent results. Thus, we decided to use normalized spectra divided by a polynomial fit to the wavelength ranges $\lambda < 3.96\,\mu$m, $3.99\,\mu{\rm m} < \lambda < 4.00\,\mu$m, $4.036\,\mu{\rm m} < \lambda < 4.040\,\mu$m, $4.076\,\mu{\rm m} < \lambda < 4.080\,\mu$m, and $\lambda > 4.115\,\mu$m, where there are no strong SiO or OH features. In this context it should be mentioned that in stars with strong SiO bands the absorption will extend into all the defined continuum regions at $\lambda > 4.0\,\mu$m, since there is no frequency not affected by SiO at our resolution. Nevertheless, this effect can easily be corrected, if one compares the data to results from theoretical calculations, as it is discussed in Sect. 4.1. Another problem may be caused by the presence of a large number of stellar water lines in the whole spectral range between 3.94 and $4.12\,\mu$m (Aringer et al. 1997b). But water absorption will only appear in the coolest objects and never become very strong. In addition, we do not expect it to change the overall slope of the continuum.

Since the stars in our sample are extremely bright in the infrared, the signal/noise ratio is always very high. In addition, almost all of the objects have been observed more than once (usually 3 to 4 times). The different spectra, which have been averaged in order to get the final data, are generally identical concerning their features. But – even after a careful reduction – there were some variable spikes produced by the detector. Because of their fixed positions the stronger ones could be easily identified and removed using the O and B stars. Nevertheless, the weak ones and those, which did not appear in the spectra of the hot objects, remain in the final data. A good example is the relatively strong spike at $3.998\,\mu$m that can be seen in some of our stars (see Fig. 1).

The normalized spectra of all objects are shown in Fig. 1. In most of them one can see the first three bandheads of the main isotope ^{28}Si^{16}O situated at $4.0042\,\mu$m (V = 2 $\rightarrow$ 0), $4.0437\,\mu$m (V = 3 $\rightarrow$ 1) and $4.0838\,\mu$m (V = 4 $\rightarrow$ 2) as the dominant feature. But there are also stars like X Hya, R Oph, RR Sgr and S Vir, all of which are Mira variables, having only a very weak or no SiO absorption. Some of them show Brackett-α emission at $4.05\,\mu$m, which is a sign for the appearance of atmospheric shock waves. The distinct depression between 3.96 and $3.99\,\mu$m is caused by OH (e.g. Decin et al. 1997). It can only be seen in objects with intense SiO bands. Finally, as it has already been mentioned, there are a lot of H_2O lines in the whole observed spectral range, which become important for the coolest stars with $T_{\rm eff} \leq 2800$ K. However, they will not give rise to any remarkable intense features (Aringer et al. 1997b). Instead, they are expected to reduce the continuum flux level and introduce many small absorption dips into the spectrum.

Isotopic bandheads of SiO are situated at $4.0292\,\mu$m (V = 2 $\rightarrow$ 0, ^{29}SiO), $4.0529\,\mu$m (V = 2 $\rightarrow$ 0, ^{30}SiO), $4.0687\,\mu$m (V = 3 $\rightarrow$ 1, ^{29}SiO), $4.0924\,\mu$m (V = 3 $\rightarrow$ 1, ^{30}SiO) and $4.1088\,\mu$m (V = 4 $\rightarrow$ 2, ^{29}SiO). According to our synthetic spectra published in Paper I, the most distinct of them are expected at 4.0687 and $4.1088\,\mu$m. Especially at the first of these positions, there is a quite strong feature that can be seen in all sources with large SiO absorption. But also the second band, which appears to be weaker, seems to be present at least in some of the stars. However, it should be noted that around 4.07 as well as around $4.11\,\mu$m an accumulation of some intense OH lines can be found (e.g. Decin et al. 1997). Thus, we assume these features to be formed by ^{29}SiO and OH together. The remaining isotopic bands are only very weak or not visible. This is especially true for ^{30}SiO, because its bandheads fall into an area with intense absorption from the main isotope. Maybe they produce small peaks seen in the spectra of some objects like SU Sgr. But that could also be due to another species like water in the earth's or stellar atmosphere. A possible exception concerning the appearance of isotopic bands is the strange spectrum of RR Aql showing intense features at all of their positions.

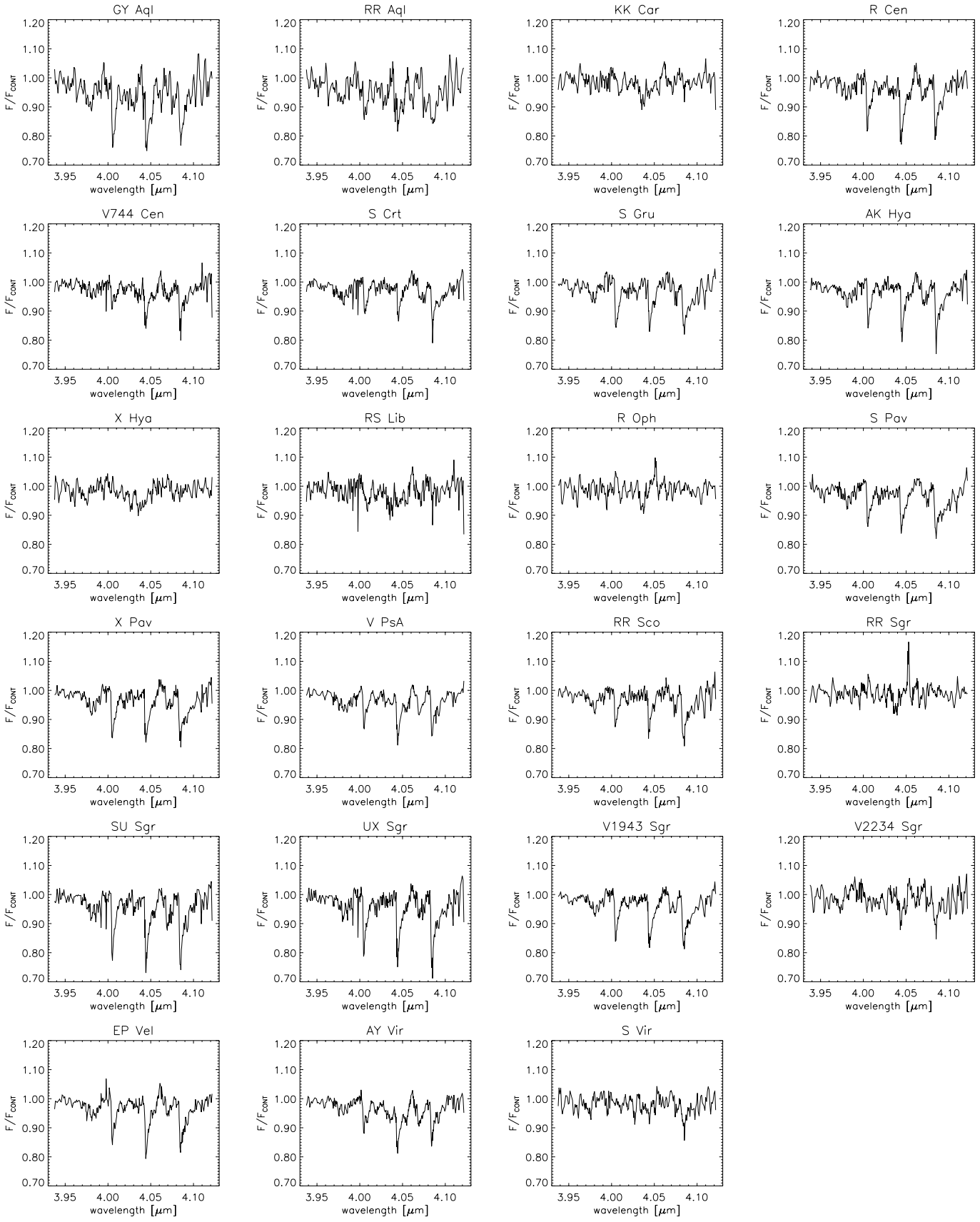

Fig. 1. Observed IRSPEC spectra of 23 AGB stars including first overtone bandheads of SiO.

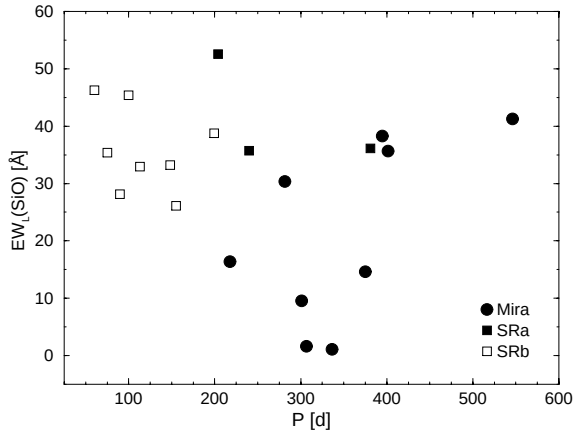

Fig. 2. $\mathrm{EW_L(SiO)}$ as a function of the photometric period for Mira, SRa and SRb stars.

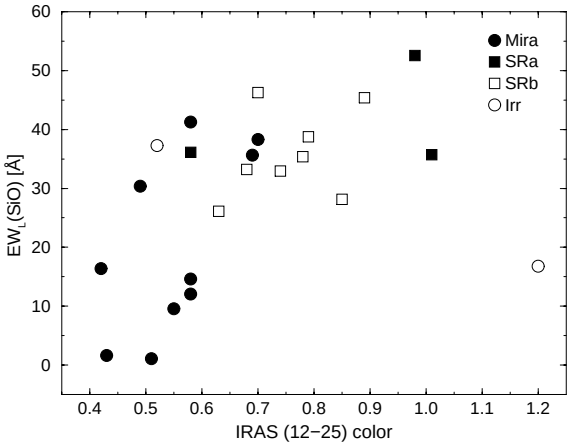

Fig. 3. $\mathrm{EW_L(SiO)}$ as a function of the IRAS (12−25) color for Mira, SRa, SRb and Irregular variables.

In order to evaluate the intensity of the SiO absorption we have measured $\mathrm{EW_L(SiO)}$, which is the sum of the equivalent widths corresponding to the V = 2 → 0, V = 3 → 1 and V = 4 → 2 bandheads of the main isotope. This has been done exactly in the same way as in Paper I for the synthetic spectra. The results are listed in Table 1. The typical uncertainty of these values, which is mainly due to the definition of the local continuum around the bandheads, amounts to ± 5 Å.

3. SiO and stellar properties

A very important attribute of most AGB stars is their pulsation. In Fig. 2 we show $\mathrm{EW_L(SiO)}$ as a function of the photometric periods listed in Table 1, which are taken from the GCVS (General Catalogue of Variable Stars). The variability types are separated using different symbols. As one can see, the Miras are located at periods longer than 200 days, whereas all SRb stars have shorter cycles. The SRa variables represent an intermediate class between those two groups (Kerschbaum & Hron 1992). It is obvious that objects with weak or no SiO absorption ($\mathrm{EW_L(SiO)} < 20$ Å) are only found among the Miras. Since there are also some of them showing quite intense bandheads ($\mathrm{EW_L(SiO)} > 30$ Å), we get a large scatter of the $\mathrm{EW_L(SiO)}$ values for the longer periods. This may be due to the spectral variability discovered by Rinsland & Wing (1982), who noticed that the SiO bands become very weak or disappear in Mira stars about the time of the visual light maximum. On the other hand, all SR objects have a large SiO absorption, which also indicates that the weak bands of the Miras are caused somehow by their strong pulsations. It should be noted that the most intense bandheads ($\mathrm{EW_L(SiO)} > 45$ Å) appear only among the SR stars of our sample. Because of the expected variability and the small number of objects with longer periods it is not sure if this represents a general trend.

For those Miras in Table 1 where periods from the GCVS as well as information on the light maxima from the AAVSO (Mattei 1996) are available we have also listed the visual phase at the time of our observations. We did not give a value for R Cen, since according to the GCVS it has two periods. Although the sample is very small, it again confirms the scenario that the SiO bands become weak or disappear around the time of the light maximum (see also Fig. 7).

Another interesting property of AGB stars is their photometric colors in the near and mid infrared. We have taken the 12, 25 and 60 μm fluxes from the IRAS-PSC (Joint IRAS Science Working Group 1988b) and combined them with near infrared measurements from Fouqué et al. (1992), Kerschbaum & Hron (1994, for EP Vel) and Catchpole et al. (1979, for R Cen). Some of the resulting colors are listed in Table 1. We did not attempt to correct the values for the effects of interstellar or circumstellar reddening. In addition, one should always bear in mind that the SiO spectra and the photometric fluxes, which are expected to be variable, have not been taken at the same time. This will introduce some scatter in all of the diagrams.

In Fig. 3 we present $\mathrm{EW_L(SiO)}$ as a function of the (12−25) color from the IRAS photometry, which mainly probes the properties of the circumstellar shell. Like in Fig. 2 the variability types are shown with different symbols. For the IRAS magnitudes we have used the definition given in the Explanatory Supplement (Joint IRAS Science Working Group 1988a). No color correction has been applied. As one can clearly see, $\mathrm{EW_L(SiO)}$ generally seems to be increasing for higher values of (12−25). This is caused by the fact that the Miras in our sample, and especially those with weak or no SiO absorption, have bluer colors than the SR variables. If one neglects the objects with $\mathrm{EW_L(SiO)} < 20$ Å, the trend will disappear. However, it is interesting that just these Miras show such blue colors. The only source which does not follow this general behaviour is the very red Irregular variable V2234 Sgr situated at a (12−25) value of 1.20. But it also deviates significantly from the rest of the objects for all other infrared colors and is probably not an AGB star.

We have also studied the SiO band intensities as a function of the (K−12) color, the latter depending very much on the thickness of the circumstellar envelope. Although the Miras are statistically redder than the SRb variables, we did not find any trend of the $\mathrm{EW_L(SiO)}$ values in the corresponding diagram.

Table 1. $EW_L(SiO)$-values, pulsational and photometric properties of the observed stars. T_{BB1} and T_{BB2} are the temperatures from a fit of two blackbodies, while $T_{(J-K)}$ corresponds to the effective temperature derived from the (J−K) color (see text).

object	EW_L [Å]	type	P [d]	(J–K)	(K–12)	(12–25)	LRS	$T_{(J-K)}$ [K]	T_{BB1} [K]	T_{BB2} [K]	Phase
GY Aql	52.6	SR	204	1.70	3.18	0.98	28		2254	451	
RR Aql	38.3	M	395	1.57	2.83	0.70	27		2418	509	0.30
KK Car	12.0	M		1.64	1.86	0.58	21		2587	554	
R Cen	41.3	M	546	1.37	2.45	0.58	22	3091	2902	739	
V744 Cen	28.2	SRb	90	1.32	1.52	0.85	22	3189	3326	505	
S Crt	26.1	SRb	155	1.34	1.51	0.63	16	3152	3097	496	
S Gru	35.7	M	402	1.33	2.52	0.69	22	3171	2807	543	0.58
AK Hya	35.4	SRb	75	1.30	1.46	0.78	22	3226	3500	479	
X Hya	9.5	M	301	1.53	1.97	0.55	15	2414	2645	586	0.16
RS Lib	16.4	M	218	1.40	2.11	0.42	15	3032	2724	573	0.93
R Oph	1.6	M	306	1.48	1.60	0.43	16	2766	2809	548	0.91
S Pav	36.1	SRa	381	1.39	1.74	0.58	14	3051	2926	584	
X Pav	38.8	SRb	199	1.45	2.07	0.79	22	2909	3005	453	
V PsA	33.2	SRb	148	1.43	1.82	0.68	22	2959	3109	497	
RR Sco	30.4	M	281	1.46	1.97	0.49	15	2884	2585	577	0.58
RR Sgr	1.1	M	336	1.32	2.67	0.51	23	3189	2712	620	0.93
SU Sgr	46.3	SRb	60	1.43	1.25	0.70	16	2959	3329	346	
UX Sgr	45.4	SRb	100	1.38	1.57	0.89	24	3071	3487	491	
V1943 Sgr	37.3	Lb		1.40	1.52	0.52	15	3032	3070	498	
V2234 Sgr	16.8	L		1.96	3.95	1.20	28		2012	397	
EP Vel	35.7	SRa	240	1.60	2.32	1.01	26		2746	442	
AY Vir	33.0	SRb	113	1.35	1.42	0.74	16	3132	3189	472	
S Vir	14.6	M	375	1.47	2.29	0.58	16	2824	2464	648	0.23

This agrees with the fact that there is also no correlation with the IRAS LRS class probing the optical depth of the dust shell. Finally, we have studied the SiO absorption as a function of the (J−K) color, which depends mainly on the stellar temperature, and we got the same behaviour as for (K−12): the Miras are statistically redder, but there is no correlation with $EW_L(SiO)$. It should be mentioned that, like in (12−25), V2234 Sgr is also extremely red in (K−12) and (J−K).

The photometric data can also be used to determine temperatures for the stars. One of the simplest methods is to fit two blackbodies to the spectral energy distribution in the near and mid infrared. They are attributed to the stellar photosphere and the circumstellar gas and dust shell, respectively (Kerschbaum & Hron 1996). Of course, neither the star nor its envelope radiate like a blackbody and this technique does not provide a direct measurement of the effective temperature. Nevertheless, the results are interesting, since they contain information on the overall spectral energy distribution. We have obtained such blackbody temperatures using the already mentioned IRAS and near infrared photometry as well as visual magnitudes published in the GCVS. But due to their large variability the latter have only been given a very low statistical weight. The temperatures for the first blackbody attributed to the stellar photosphere (T_{BB1}) are listed in Table 1. Their typical uncertainty being mainly due to stellar variability is about $\pm 100\,K$. A plot of the $EW_L(SiO)$ values versus T_{BB1} is shown in Fig. 4a. There one can see that the Miras in our sample generally have lower blackbody temperatures than the SRb stars. As a consequence objects

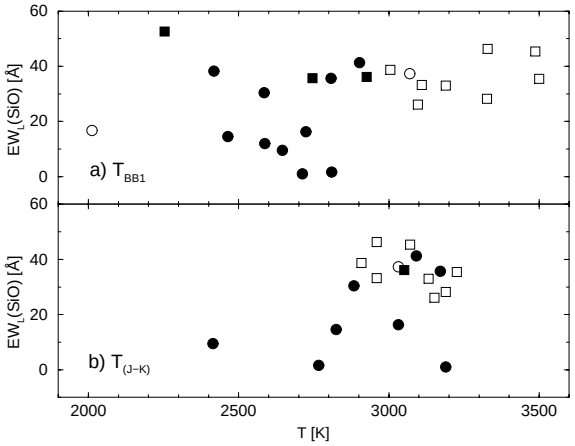

Fig. 4a and b. $EW_L(SiO)$ as a function of the first blackbody temperature (T_{BB1}, **a**) and the effective temperature derived from the (J−K) color ($T_{(J-K)}$, **b**) for Mira, SRa, SRb and Irregular variables. A detailed explanation concerning the definition of these temperatures is given in the text. The symbols for the variability types are as in Fig. 3.

with weak or no SiO absorption appear only at $T_{BB1} < 2900\,K$ and for the cooler sources there seems to be a large scatter in the diagram, whereas all hotter objects have more intense bands. It should be mentioned that in stars with $T_{BB1} < 2300\,K$ the first blackbody may be strongly affected by the circumstellar shell.

In order to determine effective temperatures from photometric data we have used a semi-empirical relation by Ng et al. (in preparation), which connects them with the (J−K) color. This

method is based on angular diameter measurements by Ridgway et al. (1980), Dyck et al. (1996) and van Belle et al. (1996). The results are shown in Table 1 and Fig. 4b. For some of the objects we could not determine a $\mathrm{T_{eff}}$-value, since they are too red for the relation. It is obvious, that there is no visible trend in the diagram. In this context it should be noted that, at least for the cooler stars in our sample, we expect large uncertainties concerning the effective temperatures. First, in extremely extended objects dominated by pulsation and mass loss the definition of such a quantity becomes problematic. This affects the interpretation of any kind of observations, which requires a detailed knowledge about the stellar atmospheres being not available at the moment (see next section). A good example is the strong wavelength dependence of the measured angular diameters of cool Miras. In addition, in dynamical models the effective temperature loses its unique role for characterizing the atmospheric structure, and thus, the observed spectrum: for a given stellar mass and chemical composition, the physics of a hydrostatic environment may be described by the gravitational acceleration and the effective temperature. But this will not work for dynamical atmospheres, since their structure is dominated by pulsation and mass loss. Another problem concerning the $\mathrm{T_{eff}}$-values listed in Table 1 is the fact that especially the cooler stars in our sample may have thick envelopes producing a considerable amount of circumstellar reddening. This could be the reason some objects are too red for the relation by Ng et al. (in preparation).

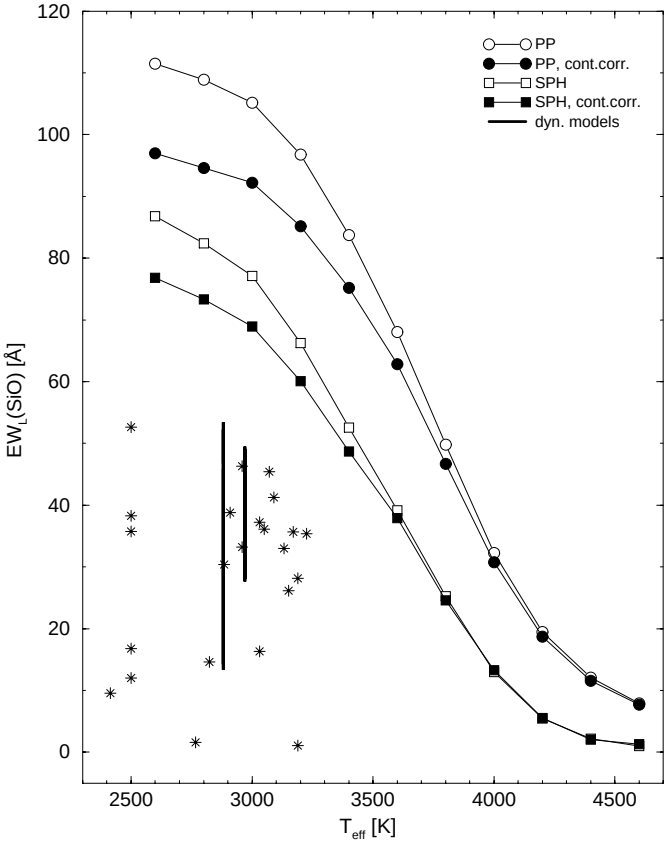

Fig. 5. $\mathrm{EW_L(SiO)}$ as a function of the effective temperature. We show four sequences based on hydrostatic spherical MARCS models with $\log(\mathrm{g}) = 0.0$, solar mass and chemical abundances: a) plane-parallel radiative transfer (open circles), b) plane-parallel radiative transfer and corrected for the influence of the SiO absorption on the observed continuum (full circles), c) spherical radiative transfer (open squares), d) spherical radiative transfer and corrected for the influence of the SiO absorption on the observed continuum (full squares); The observed $\mathrm{EW_L(SiO)}$-values are displayed as stars. The corresponding effective temperatures are derived from the (J−K) color. We have also included the ranges of equivalent widths covered by the two dynamical atmospheres p5t297solu2 and p5t288solu2, which are shown as vertical lines at the temperatures of the hydrostatic initial models.

4. Synthetic spectra

4.1. Hydrostatic atmospheres

One of the main conclusions in Paper I was that our synthetic spectra based on hydrostatic MARCS atmospheres are able to reproduce the SiO bands of K and early M giants, but they fail to explain the relatively weak features seen in very cool and extended stars. Instead, they predict a monotonic increase of the equivalent width with lower temperature and surface gravity. This problem is clearly illustrated by the objects in our sample. If one compares the $\mathrm{EW_L(SiO)}$- and $\mathrm{T_{eff}}$-values listed in Table 1 with the theoretical results, one finds that even the most intense of the observed bands are at least a factor of two weaker than expected from the synthetic spectra for $\log(\mathrm{g[cm/s^2]}) = 0.0$. The situation only becomes worse for the Mira variables with weak or no SiO absorption and for more extended models. The discrepancy is demonstrated in Fig. 5 where the observations (stars) as well as the original theoretical $\mathrm{EW_L(SiO)}$-values derived for atmospheres with $\log(\mathrm{g[cm/s^2]}) = 0.0$ (uppermost curve with open circles) are shown. For the stars being too red for the $\mathrm{T_{eff}}$ versus (J−K) relation from Ng et al. (in preparation) we have adopted $\mathrm{T_{eff}} = 2500\,\mathrm{K}$, which is between the coolest hydrostatic models (2600 K) and the smallest $\mathrm{T_{(J-K)}}$ value found in Table 1 (2414 K). In this context it should be noted that the discrepancies cannot be caused by the uncertainty of the effective temperatures discussed in the previous section. In order to follow the theoretical predictions all objects in our sample must be at least hotter than 3600 to 3800 K, depending on their surface gravity. For the stars with weak or no SiO absorption one would even need $\mathrm{T_{eff}}$-values much larger than 4000 K. All of this is not realistic. Thus, we have to conclude that the synthetic spectra published in Paper I really fail to reproduce the SiO bands of the observed objects presented in this work. However, Paper I was not dedicated to AGB stars and if one wants to study very extended sources showing strong SiO absorption the theoretical treatment should be improved for two reasons:

First, as it is described in Sect. 2, the observed spectra have been normalized using a polynomial fit to wavelength regions which do not contain any prominent SiO or OH features. In contrast, the equivalent widths published in Paper I are based on the theoretical stellar continuum corresponding to a radiative transfer calculation without molecular or atomic lines. Both methods will give similar results as long as the SiO bands remain

relatively weak ($\mathrm{EW_L(SiO)} < 50$ Å). But if the SiO absorption becomes more intense, it affects all those spectral intervals used for the polynomial fit, which are situated at $\lambda > 4.0\,\mu$m. This effect can already be seen in the synthetic spectrum of an object with $\mathrm{T_{eff}} = 3600$ K, solar mass and $\log(\mathrm{g[cm/s^2]}) = 0.0$ as it is shown in the first figure of Paper I, although it gets much stronger for cooler stars. It depends on the resolution and causes the local continuum derived from the observations to be steeper and at a lower level than the theoretical one. As a consequence the measured equivalent widths will decrease considerably. In order to take this effect into account when comparing the theoretical predictions with the objects in our sample we have rebinned the synthetic spectra to the same resolution as the observed ones and then we normalized them to the same kind of pseudo-continuum (polynomial fit). The results can be seen in Fig. 5 where we show the temperature sequence of the original (open circles) and the continuum corrected (full circles) $\mathrm{EW_L(SiO)}$-values for models with $\log(\mathrm{g[cm/s^2]}) = 0.0$, solar mass and chemical abundances. As it is demonstrated in the diagram the total equivalent width of the SiO bands decreases in the coolest stars by approximately 15%.

The second improvement that has to be applied to the predicted equivalent widths is connected to sphericity. In principle, the results published in Paper I are based on atmospheric structures derived from spherical calculations (MARCS code with spherical routines from Nordlund 1984). However, for the subsequent computation of the synthetic spectra a plane-parallel radiative transfer was used. As it turned out, this approach introduces errors, which are much larger than we had expected. Especially for the very extended objects the equivalent widths will decrease significantly, if the spectra are calculated using a spherical code. This is demonstrated in Fig. 5 where we present $\mathrm{EW_L(SiO)}$-values for our standard sequence of stars with $\log(\mathrm{g[cm/s^2]}) = 0.0$, which are derived from the results of a spherical radiative transfer program (Windsteig et al. 1997, open squares). As one would expect the differences become larger with higher temperature and, of course, with lower surface gravity. For the very extended objects they are even big enough to invert the relation found in Paper I that $\mathrm{EW_L(SiO)}$ monotonically grows with decreasing values of log (g).

In Fig. 5 we also show the final temperature sequence, which results after correcting for both of the two discussed effects (full squares). It is obvious that the total equivalent widths of the SiO bands have decreased significantly, and consequently they are much closer to the highest values derived from our observations. The situation becomes even better, if one takes the uncertainties concerning the effective temperatures into account. In addition, as it has just been mentioned, we found for the very extended objects that the SiO features get weaker at lower surface gravities. For example, in a model with $\log(\mathrm{g[cm/s^2]}) = -0.5$ the value of $\mathrm{EW_L(SiO)}$ is 5 to 15 Å smaller than at $\log(\mathrm{g[cm/s^2]}) = 0.0$, depending on temperature. Thus, we can conclude that after correcting for the effect of the SiO absorption on the observed continuum and using a spherical radiative transfer for the spectrum synthesis the hydrostatic MARCS atmospheres are in principle able to explain those stars in our sample, which have the most intense SiO bands ($\mathrm{EW_L(SiO)} > 40$ Å). Of course, as it was already shown in Paper I, these models are very successful in reproducing the observed band intensities of giants with spectral types earlier than about M5 III and M2 II. Nevertheless, they still fail to reproduce the SiO spectra of all AGB stars with weaker or no features, most of which are Miras.

4.2. Dynamical atmospheres

Up to now we have calculated our synthetic spectra for AGB stars based only on hydrostatic atmospheres. This is problematic, since these objects are dominated by such phenomena as strong pulsations creating shock waves, dust formation and mass loss. All of those processes can be successfully simulated by dynamical models as they have been developed by Fleischer et al. (1992), Höfner & Dorfi (1997) or Höfner et al. (1998). The atmospheric structure there is obtained by solving the equations of grey radiation hydrodynamics together with a time-dependent description of the dust formation. The stellar pulsation is introduced as a variable boundary located beneath the photosphere moving sinusoidally with a velocity amplitude $\Delta \mathrm{u_P}$ and a period P (piston). The calculation is started with a hydrostatic initial model characterized by its effective temperature ($\mathrm{T_*}$), luminosity ($\mathrm{L_*}$) and mass ($\mathrm{M_*}$). Since the original models were mainly designed to understand the behaviour of circumstellar shells and mass loss caused by dust driven winds of carbon stars, we had to modify them slightly for our purpose:

First, for the earlier computations (e.g. Höfner & Dorfi 1997, Fleischer et al. 1992) a constant value of the gas opacity independent of thermodynamical conditions and chemical composition has been used as it was introduced in the work of Bowen (1988). However, it turns out that this assumption generally produces completely unrealistic molecular spectra (Höfner et al. 1998), since the density at a given temperature may be orders of magnitude too large, which will also change the derived mass loss rates significantly. As a consequence, we have calculated our atmospheres using Planck mean absorption coefficients for the gas opacity in an environment with solar chemical abundances. Although this is still a somewhat crude approximation, the agreement with the results from detailed frequency-dependent computations in the hydrostatic limit case is already much better. This method, its advantages and problems are discussed in Höfner et al. (1998).

The second modification is connected to the circumstellar dust shell. In contrast to the carbon stars, no applicable self-consistent description of the formation and growth of grains in an oxygen-rich environment is available at the moment. As a consequence, we did not include any dust in our models. However, we do not expect this to be a large problem concerning the atmospheric structure, since it will only have strong effects in the outer regions, where the temperatures are already low enough that solid particles can be created. On the other hand, almost all of the SiO absorption comes from layers situated much closer to the star. Exactly the same argument applies to the depletion of gaseous SiO caused by the dust formation: it happens in regions of the atmosphere which do not contribute significantly

to the observed 4 μm-bands. We have checked this by assuming that all SiO condenses into solid particles at $\mathrm{T} < 1500\,\mathrm{K}$. Although this is already a quite high temperature (e.g. Sedlmayr 1997), we found only very small changes of the resulting synthetic spectra. However, a thick dust shell might also influence the observed 4 μm-spectra through its continuous opacity. Thus, one should be careful, if one applies our results to objects with high mass loss rates, although we did not find any correlation of the SiO bands with quantities probing the optical depth of the circumstellar envelope (Sect. 3).

In order to obtain synthetic spectra based on the given dynamical atmospheric structures we have computed chemical abundances as well as continuous and SiO opacities in each layer. This is done by a program named COMA (Copenhagen Opacities for Model Atmospheres). The routines for the equilibrium chemistry and the continuum absorption are taken from a version of the MARCS code that has already been used for the construction of the hydrostatic models in Paper I (Gustafsson et al. 1975, Jørgensen et al. 1992). The SiO opacities are derived from the linelist prepared by Langhoff & Bauschlicher (1993) assuming Doppler profiles and a microturbulence of $2.5\,\mathrm{km\,s^{-1}}$ (for details see Paper I). The results of COMA are then used as an input for a spherical radiative transfer program (Windsteig et al. 1997) producing the synthetic spectra.

Up to now we have only calculated spectra for a very small number of dynamical models. In addition, one should not forget that there are still problems concerning their construction like the grey radiative transfer or the neglecting of dust in an oxygen-rich environment. Nevertheless, the first results look promising as it can be seen in Fig. 5, where we present the ranges of $\mathrm{EW_L(SiO)}$-values covered by the two atmospheres p5t297solu2 and p5t288solu2 during their pulsation cycle. They are shown as vertical lines situated at the effective temperatures of the corresponding hydrostatic initial models. The parameters for p5t297solu2 are $\mathrm{T_*} = 2970\,\mathrm{K}$, $\mathrm{L_*} = 5000\,\mathrm{L_\odot}$, $\mathrm{M_*} = 1\,\mathrm{M_\odot}$, P = 295 d and $\Delta \mathrm{u_P} = 2\,\mathrm{km\,s^{-1}}$. p5t288solu2 differs only by its $\mathrm{T_*}$, which is 2880 K. It is obvious that the observed and predicted band intensities are in good agreement, and it becomes possible to explain the spectra of Mira variables with weak or no SiO absorption.

As an example we compare in Fig. 6 the observation of S Gru with a synthetic spectrum calculated from p5t288solu2 at phase 0.4 (bolometric). Taking into account that the dynamical atmosphere was not computed to fit the stellar parameters of S Gru and that only SiO is included into the molecular opacity, the agreement is quite good. Fig. 6 also shows a spectrum derived from a MARCS model with $\mathrm{T_{eff}} = 2800\,\mathrm{K}$, $\log\left(\mathrm{g[cm/s^2]}\right) = 0.0$, solar mass and chemical abundances. Although it is calculated using a spherical radiative transfer and normalized to the same pseudo-continuum as the observations, the SiO bands are much too intense. The main reason, why the dynamical models generally predict weaker SiO features than the hydrostatic ones, is their much larger extension producing emission components in the lines. As a function of the radius, the density, and thus the partial pressure of SiO, does not decrease exponentially, and in the presence of strong pulsations even not monotonically.

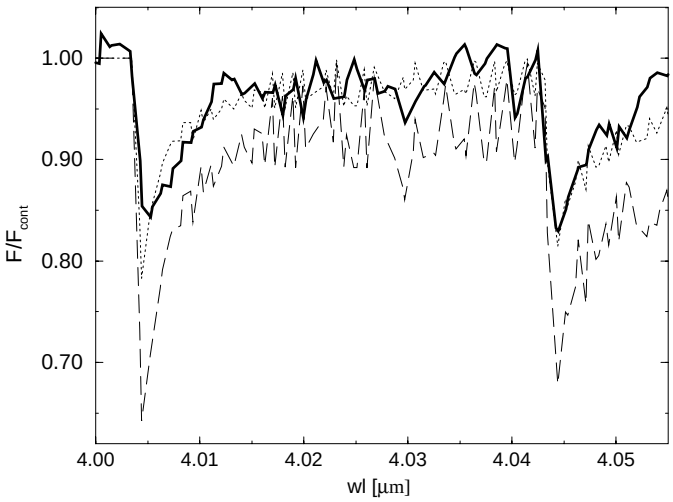

Fig. 6. The spectrum of S Gru (full line) is compared with two synthetic spectra based on the dynamical atmosphere p5t288solu2 at phase 0.4 (bolometric, dotted line) and a MARCS model with $\mathrm{T_{eff}} = 2800\,\mathrm{K}$, $\log\left(\mathrm{g[cm/s^2]}\right) = 0.0$, solar mass and chemical abundances (dashed line), respectively. The V = 2 $\rightarrow$ 0 and V = 3 $\rightarrow$ 1 bandheads of the main SiO isotope are shown. The synthetic spectra are calculated using a spherical radiative transfer and normalized to the same pseudo-continuum as the observations.

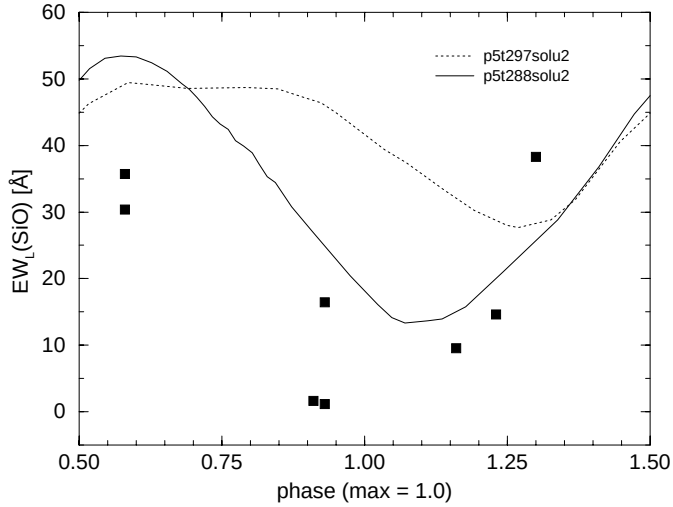

Fig. 7. $\mathrm{EW_L(SiO)}$ as a function of the bolometric phase for the two dynamical atmospheres p5t297solu2 (dotted) and p5t288solu2 (solid) and as a function of the visual phase for the Miras from Table 1 (squares).

In Fig. 7 we present $\mathrm{EW_L(SiO)}$ calculated from the dynamical atmospheres as a function of the bolometric phase. In addition we show the values for the Miras listed in Table 1. Especially p5t288solu2 seems to reproduce the observed trend that the SiO bands become weak or disappear around the time of the light maximum very well, while for p5t297solu2 the minimum of the SiO absorption happens later. However, the SiO spectra derived from the dynamical models do not show a strictly periodic behaviour (roughly periodic with perturbations) and we

expect small shifts between the visual and the bolometric phase (up to 0.1).

It should be noted that the behaviour of the SiO bands depends very much on the value of Δu_P. We have calculated spectra from models characterized by the same parameters as those in Fig. 5 except for $\Delta u_P = 3$ and $4\,\mathrm{km\,s^{-1}}$. It turned out that these atmospheres produce a considerable SiO emission during some phases of their pulsation cycle, which does not agree with the observations.

5. Conclusions

We found that in contrast to the SRb stars in our sample the Miras show a very large scatter of the equivalent widths of the SiO bandheads at $4\,\mu$m. Despite their cool temperatures some of them have only weak or no SiO absorption. This seems to be related to their strong pulsations producing a large variability of the bands, which has already been observed by Rinsland & Wing (1982).

When comparing the $\mathrm{EW_L(SiO)}$-values with other stellar properties we found that there is a general decrease with longer pulsation period, bluer IRAS (12−25) color and maybe with a cooler temperature of the first blackbody from a fit to the overall energy distribution, which is attributed to the photosphere. However, all of these trends may only reflect the different properties of the Miras and SRb stars in our sample. We did not discover any correlation of the SiO band intensities with the effective temperatures derived from (J−K), or with the (K−12) color and the IRAS-LRS class, both of which can be regarded as a rough measure for the thickness of the circumstellar shell. But in this context it should be kept in mind that our sample of objects is quite small and all statistical results will be affected by the strong variability of the SiO bands in Mira stars. Thus, it is necessary to confirm this work with a larger number of $4\,\mu$m spectra and to complement it using time-dependent observations as they have been obtained by the ISO-SWS (e.g. Hron et al. 1998).

In order to reproduce the SiO bands of very cool and extended objects, as they are discussed in this work, one has to use spherical radiative transfer based on a spherical model structure. In addition, the influence of the SiO absorption on the definition of a pseudo-continuum must be taken into account. We want to emphasize again that these two things are not important for more compact and warmer stars like M dwarfs and early M giants, where we found a good agreement between the predictions made in Paper I and the observations (see Paper I). Nevertheless, even after including sphericity into the spectral synthesis and correcting for the SiO absorption in the continuum points the spectra calculated from hydrostatic MARCS atmospheres are only able to explain the objects in our sample with the most intense SiO features ($\mathrm{EW_L(SiO)} > 40$ Å). They fail completely when it comes to Miras with weak or no SiO bands. However, these stars are dominated by dynamical phenomena and consequently they cannot be described by hydrostatic structures.

Our dynamical atmospheres still have some shortcomings like a grey radiative transfer or the somewhat artificial simulation of the pulsation as a sinusoidally moving piston at the inner boundary. In addition, at the moment the models exist only for a limited number of combinations of stellar parameters. Nevertheless, we have shown that in principle they are able to explain the whole range of equivalent widths of the observed SiO bandheads and their variations.

Thus, we conclude that hydrostatic atmospheres cannot explain the SiO bands of cool extended giants without introducing additional features, which are not part of the self-consistent solution (like the "warm molecular envelope" proposed by Tsuji et al. 1997). In contrast, the dynamical models do not need such assumptions to reproduce the observations. In the future it will therefore be very important to develop more realistic dynamical atmospheres to understand the complex relation between fundamental stellar parameters, pulsation, mass loss, dust formation and the observed spectra.

Acknowledgements. This work was supported by the Austrian Science Fund Projects S7308–AST, S7305–AST and J1487-PHY.

References

Alvarez R., Mennessier M.O., Barthés D., Luri X., Mattei J.A., 1997, A&A 327, 656
Aringer B., Wiedemann G., Käufl H.U., Hron J., 1995, Ap&SS 224, 419
Aringer B., Jørgensen U.G., Langhoff S.R., 1997a, A&A 323, 202 (Paper I)
Aringer B., Kerschbaum F., Jørgensen U.G., et al.,1997b, In: Heras A.M., Leech K., Trams N.R., Perry M. (eds.) Proc. First ISO Workshop on Analytical Spectroscopy, ESA-SP 419, p. 249
Bowen G.H., 1988, ApJ 329, 299
Catchpole R.M., Robertson B.S.C., Lloyd Evans T.H.H., et al., 1979, South African Astron. Obs. Circ. 1, 61
Decin L., Cohen M., Eriksson K., et al., 1997, In: Heras A.M., Leech K., Trams N.R., Perry M. (eds.) Proc. First ISO Workshop on Analytical Spectroscopy, ESA-SP 419, p. 185
Dyck H.M., Benson J.A., van Belle G.T., Ridgway S.T., 1996, AJ 111, 1705
Fleischer A.J., Gauger A., Sedlmayr E., 1992, A&A 266, 321
Fouqué P., Le Bertre T., Epchtein N., Guglielmo F., Kerschbaum F., 1992, A&AS 93, 151
Gail H.P., Sedlmayr E., 1986, A&A 166, 225
Gustafsson B., Bell R.A., Eriksson K., Nordlund Å., 1975, A&A 42, 407
Höfner S., Dorfi E.A., 1997, A&A 319, 648
Höfner S., Jørgensen U.G., Loidl R., Aringer B., 1998, A&A 340, 497
Hron J., Loidl R., Höfner S., et al., 1998, A&A 335, L69
Joint IRAS Science Working Group, 1988a, IRAS Catalogs and Atlases. Vol. 1, Explanatory Supplement, NASA RP–1190
Joint IRAS Science Working Group, 1988b, IRAS Catalogs and Atlases. Vol. 2–6, The Point Source Catalog, NASA RP–1190
Jørgensen U.G., Johnson H.R., Nordlund Å., 1992, A&A 261, 263
Kerschbaum F., Hron J., 1992, A&A 263, 97
Kerschbaum F., Hron J., 1994, A&AS 106, 397
Kerschbaum F., Hron J., 1996, A&A 308, 489
Langhoff S.R., Bauschlicher C.W., 1993, Chem. Phys. Lett. 211, 305
Loidl R., Hron J., Höfner S., et al., 1997, Ap&SS 251, 243
Mattei J.A., 1996, AAVSO Bull. 60

Nordlund Å, 1984, In: Kalkofen W. (ed.) Methods in Radiative Transfer. Cambridge University Press, Cambridge, p. 211
Ridgway S.T., Joyce R.R., White N.M., Wing R.F., 1980, ApJ 235, 126
Ridgway S.T., Carbon D.F., Hall D.N.B., Jewell J., 1984, ApJS 54, 177
Rinsland C.P., Wing R.F., 1982, ApJ 262, 201
Sedlmayr E., 1997, Ap&SS 251, 103
Tsuji T., Ohnaka K., Hinkle K.H., Ridgway S.T., 1994, A&A 289, 469
Tsuji T., Ohnaka K., Aoki W., Yamamura I., 1997, A&A 320, L1
van Belle G.T., Dyck H.M., Benson J.A., Lacasse M.G., 1996, AJ 112, 2147
Windsteig W., Dorfi E.A., Höfner S., Hron J., Kerschbaum F., 1997, A&A 324, 617